Hindawi
International Journal of Antennas and Propagation
Volume 2024, Article ID 4236695, 10 pages
https://doi.org/10.1155/2024/4236695

Research Article

All-Textile Compact Ultra-Wideband Microstrip Antenna with Full Ground Plane for WBAN Applications

Jinxin Du,[1] **Ruimeng Wang**,[1] **Haiyan Li**,[2] **Xue-Xia Yang**,[2] **and Christophe Roblin**[3]

[1]*Sino-European School of Technology, Shanghai University, Shanghai 200444, China*
[2]*The Key Laboratory of Specialty Fiber Optics and Optical Access Networks, Shanghai University, Shanghai 200444, China*
[3]*LTCI, Télécom Paris, Institut Polytechnique de Paris, Palaiseau 91123, France*

Correspondence should be addressed to Xue-Xia Yang; yang.xx@shu.edu.cn

Received 20 June 2023; Revised 20 October 2023; Accepted 22 January 2024; Published 27 January 2024

Academic Editor: Hervé Aubert

A novel low-profile all-textile microstrip antenna for ultra-wideband (UWB) applications in wireless body area networks (WBANs) is presented. The antenna incorporates flexible materials such as felt and conductive fabrics which provide optimal wearing comfort and durability. The use of a single dielectric substrate layer facilitates the integration process. The antenna also features a full background plane that minimizes the back radiation towards the human body. Multiple branches are designed in a compact area to generate adjacent resonances, and their combination achieves broadband characteristics across the 4.83–9.57 GHz frequency band. The antenna has a miniaturized size of 60 mm × 60 mm, which is $1.6\lambda_g \times 1.6\lambda_g$ (where λ_g represents the guided wavelength at the center frequency), and it has a high realized gain of up to 10 dBi. The fully grounded structure also ensures good isolation between the antenna and the human body, thereby alleviating concerns regarding safety and radiation degradation in WBAN context. Simulation results indicate that the antenna maintains high performance levels during various bending tests. Given its favourable properties like ultra-wide bandwidth, compact size, low profile, high flexibility, and low specific absorption rate (SAR), the proposed design could find broad application prospects in high-speed WBAN systems.

1. Introduction

With the rapid development of wireless communication, wearable materials, and sensor technologies, the wireless body area network (WBAN) has gained popularity in diverse fields including military activities, sports, healthcare, emergency rescue, and personal communications [1–5]. The antenna, as a crucial component enabling wireless transmission, requires thorough design to address challenges such as wearing comfort, high-speed transmission, safety, and cost-effectiveness. On the one hand, all-textile antennas offer a promising solution for better conformability, breathability, and aesthetics compared to their counterparts made from semirigid printed circuit board (PCB) or flexible polyester rubbers. The manufacturing techniques for textile antennas are also becoming increasingly mature and diversified, such as wet corrosion, manual cutting, laser cutting, screen printing, ink-jet printing, and embroidery [6, 7]. However, effectively integrating multiple fabric layers while avoiding detachment and dislocation between them still poses challenges. Reducing the number of dielectric and conductive layers can alleviate these difficulties. On the other hand, ultra-wideband (UWB) technology is desirable for high-speed data transfer, low power consumption, and strong anti-interference robustness. In addition, since human tissue is rich in water and consequently can serve as a good absorber, reflector, or scatterer of electromagnetic (EM) waves, effective insulation or shielding measures become necessary to minimize the interference between the human body and the antenna and prevent potential negative even harmful radiation impacts [8]. Wearable antennas should also keep steady radiation performance in complex conditions such as bending and humidity environment [9, 10]. In short, for short-range and high-speed WBAN

applications, there is an increasing demand for low-profile all-textile UWB planar antennas with good back-shielding characteristic.

According to the shielding ability they have, UWB antennas reported from the existing literature can be categorized into three types. These include UWB antennas with partial ground plane, UWB antennas with electric band gap (EBG) structure or artificial magnetic conductor (AMC) structure, and UWB antennas with full ground plane.

Partially grounded antennas can achieve UWB characteristic with simple topologies [11–14]; however, their shielding performance is quite limited. When implemented near the human body, they often exhibit severe radiation distortion and can lead to high SAR values. To ensure personal safety, people tend to limit the radiation power of the antenna and maintain a thick gap between the antenna and the human body, which significantly restricts their application. To mitigate the interference between the antenna and the human body, a plane layer with periodic EBG or AMC structure can be added beneath the radiating antenna [15–18]. These structures also contribute to improved gain and radiation efficiency due to the *in-phase* reflection effects. The main deficiencies are the high overall thickness and the large surface area, since EBG or AMC structures must contain a sufficient number of periodic elements. Furthermore, the integration of multiple layers is also challenging, and small misalignments between layers may cause significant degradation in radiation when placed on the human body. In contrast, a fully grounded antenna does not introduce additional layers and has good shielding properties. However, the EM waves are inherently confined between the radiator and the ground plane, and only those around the resonance can effectively radiate, hence resulting in generally very narrow-band characteristics, such as the design in [19]. Extending the bandwidth of a fully grounded design is a challenge that has not been fully studied.

Several recent developments in fully grounded UWB antennas can be found in [20–25]. In [20], Poffelie et al. proposed an all-textile UWB antenna with two stacked substrate layers. The main radiating element is a partially grounded coplanar waveguide- (CPW-) fed patch, with a second substrate layer attached by sewing that is fully grounded to ensure good shielding. A parasitic patch is placed on the upper side of the second substrate layer just beneath the radiating patch to further expand the bandwidth. It covers the entire UWB 3.1–10.6 GHz band, but the only drawback is the high thickness and risks to introduce air gap between substrate layers under bending or crumpling conditions. In [21, 22], single-substrate-layer UWB designs are proposed using the multibranch/slot loading techniques and multiple TM mode excitation techniques, respectively. However, both designs adopt polydimethylsiloxane (PDMS) polymer as the dielectric layer, which hinders the breathability and wearing comfort. In [23], an extremely compact textile antenna is realized using the slot loading technique, while there is a large stop-band (4.2–6.5 GHz) in the middle. In [24], a multiresonance overlapped ultra-wideband width of 3.6–10.3 GHz is achieved thanks to three independent radiating branches and a surrounding patch that enables capacitive coupling, but its overall size is as large as $2.7\lambda_g \times 2.45\lambda_g$. In [25], a multiband antenna operating at both the 4.5–10 GHz UWB and the 2.45 GHz WLAN is realized using capacitive coupling techniques. The design measures as large as $2\lambda_g \times 1.75\lambda_g$ and is moderately breathable since foam instead of textile material was used as the substrate.

In this paper, we propose a highly compact all-textile ultra-wideband antenna suitable for high-speed WBAN off-body communication. Multiple radiating branches are combined to achieve adjacent resonance overlap, while a full ground plane ensures superior immunity to body proximity effects. The use of fully textile flexible materials results in good unobtrusiveness and wearing comfort.

2. Materials and Methods

Figures 1(a) and 1(b) show the topology, and Figure 1(c) shows the fabricated prototype of the proposed design. The substrate is made of 3.2 mm thick felt with a dielectric constant (ε_r) of 1.2 (measured by using the resonance method in [26]) and a loss tangent (tanδ) of 0.02 (measured by using the microstrip ring resonator method in [27]). The radiating patch and ground plane are made of flexible conductive fabric, which is a plain-weave polyester fiber layer with copper and nickel coated on the upper surface, and a very thin adhesive layer attached to the bottom to facilitate integration onto the substrate [28]. It has a thickness of 0.085 mm and a very low sheet resistance of less than 0.05 Ω/sq. The conductive and dielectric layers are processed and integrated using the manufacturing method proposed in [29]. A coaxial feeding is used, and the design parameters are as follows: $L_1 = 21.2$, $L_2 = 20$, $L_3 = 16.5$, $L_4 = 22.5$, $L_5 = 13.2$, $L_6 = 10.5$, $L_7 = 20$, $W_1 = 47$, $W_2 = 34$, $wf_1 = 6$, $wf_2 = 8$, and $h = 3.2$, all in millimeters. The overall size is $60 \times 60 \times 3.37\ \text{mm}^3$, which is $1.6\lambda_g \times 1.6\lambda_g \times 0.08\lambda_g$ (where λ_g is the guided wavelength at the center frequency).

Figures 2(a)–2(d) depict the evolutionary design process. Antenna 1, a half-wavelength rectangular patch antenna, serves as the starting point, with a resonance frequency around 6 GHz. Two L-shaped branches are added to the left and right sides to obtain antenna 2, introducing a new resonance point around 5 GHz. The middle branch's higher-order mode is excited to generate another new resonance at 9.28 GHz, while the original resonance at 6 GHz is shifted to a higher frequency of 6.4 GHz. Antenna 3 is loaded with two L-shaped stubs above antenna 2, creating additional resonances at 5.76, 7.23, and 8.13 GHz. Two elliptical cuts and a circular slot are introduced separately on the upper and lower stubs to achieve better impedance matching. To expand the bandwidth further, another rectangular stub is added to the middle of the upper half of the patch in antenna 4, creating a new resonance at 9.1 GHz. Finally, the overlapped frequency band, in which the reflection coefficient $|S_{11}| \leq -10$ dB, covers 4.89–9.65 GHz, as shown in Figure 3. Figures 4(a)–4(f) show the surface current of the final design at six resonant frequencies of 5.06, 5.76, 6.49, 7.24, 8.46, and 9.1 GHz. We can identify their corresponding current path. The length of the current paths is approximately half the

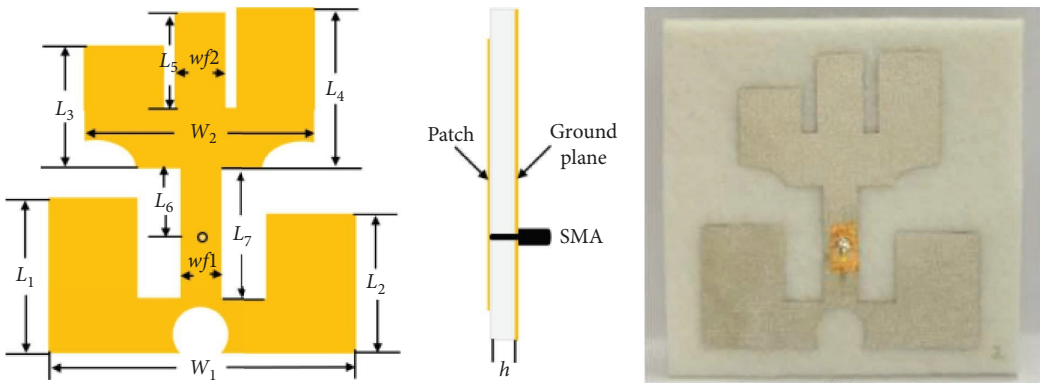

(a) (b) (c)

Figure 1: The proposed UWB design: (a) geometric topology (main view), (b) geometry topology (side view), and (c) prototype.

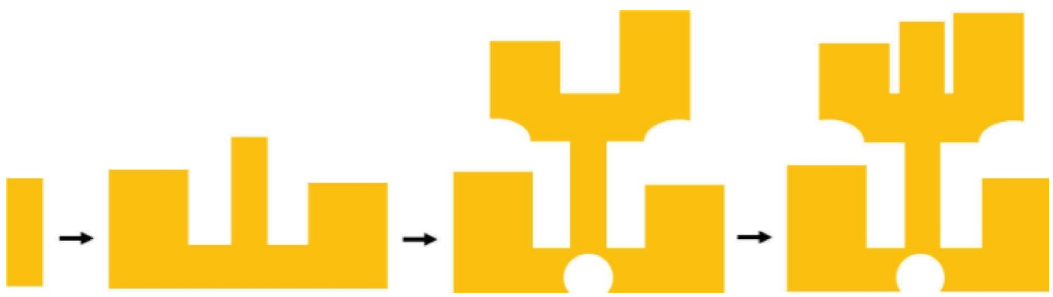

(a) (b) (c) (d)

Figure 2: Evolution of the antenna design: (a) antenna 1, (b) antenna 2, (c) antenna 3, and (d) antenna 4.

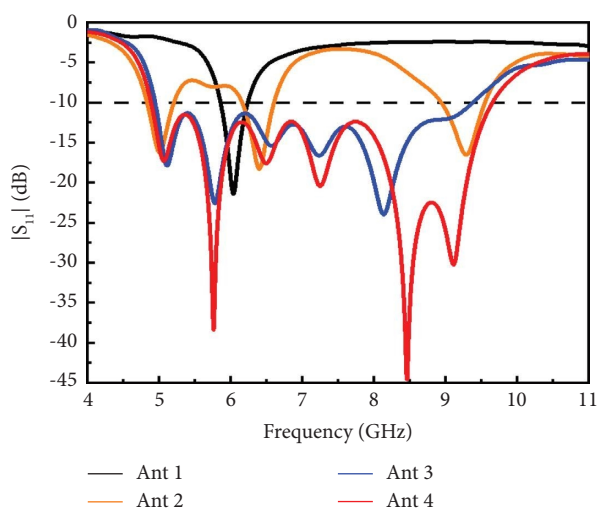

Figure 3: Reflection coefficient of the antenna designs (simulation results by CST).

waveguide wavelength at their corresponding resonant frequency. Superposition or cancellation of far-field radiation occurs when there are multiple current paths at the same frequency. This results in enhancement or splitting of the radiation pattern.

3. Results and Discussion

3.1. Bandwidth. To validate the proposed design, a proof-of-concept all-textile prototype was fabricated. The reflection coefficient $|S_{11}|$ of the antenna was measured using a vector

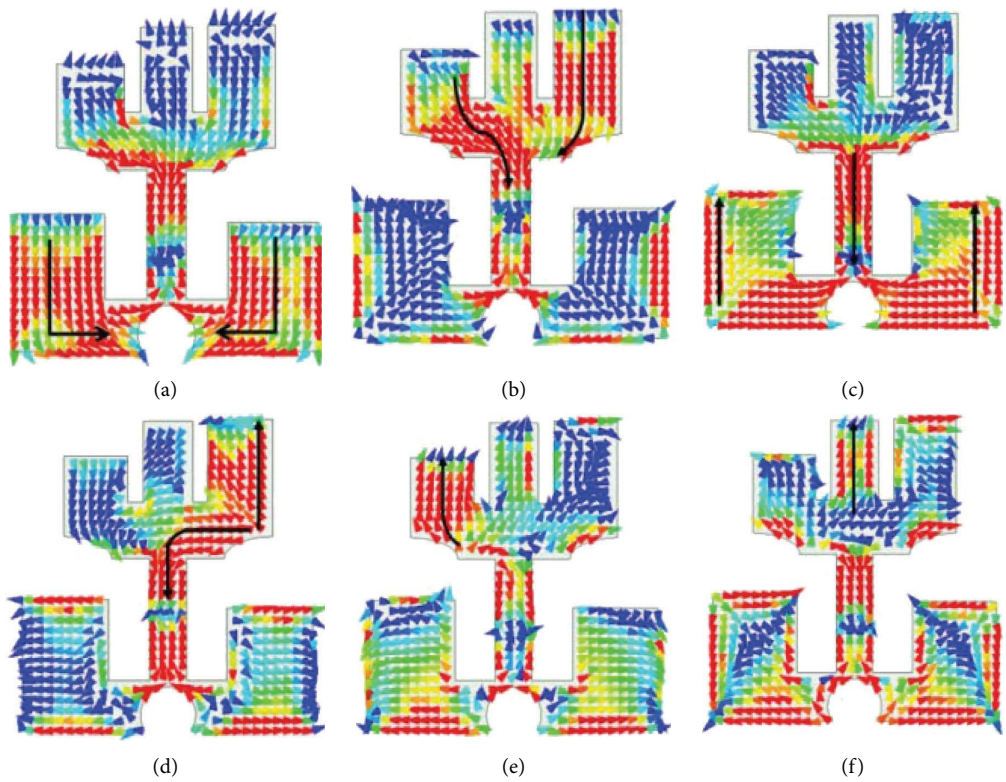

Figure 4: Distribution of the surface current of the final design at (a) 5.06 GHz, (b) 5.76 GHz, (c) 6.49 GHz, (d) 7.24 GHz, (e) 8.46 GHz, and (f) 9.1 GHz.

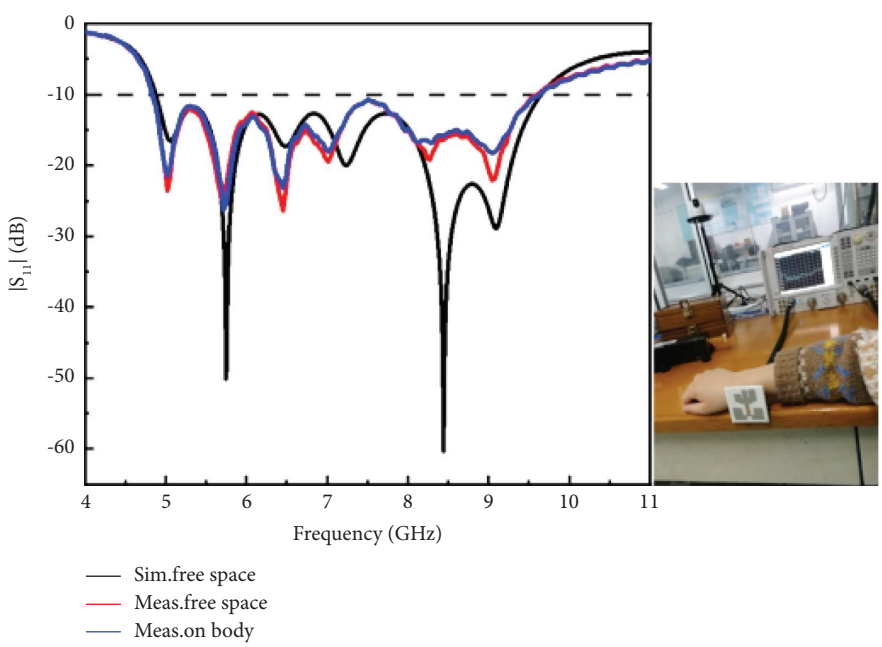

Figure 5: Simulated and measured $|S_{11}|$ of the planar antenna in free space or on body.

network analyzer and compared with the values obtained from the full-wave simulation software CST 2019. Figure 5 depicts the reflection coefficients of the antenna when placed in free space or on the human body. In free space, the simulated and measured bandwidths cover the 4.89–9.65 GHz and 4.83–9.57 GHz bands, respectively. The measured resonances are slightly shifted towards lower frequencies, which may be due to slight inaccuracies in permittivity measure. Another possible explanation could be that the textile substrate, when exposed to open space,

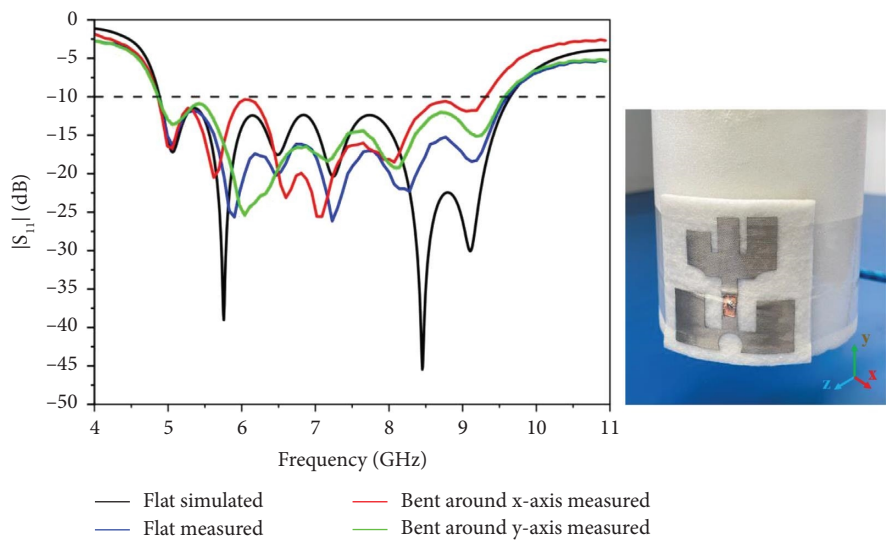

Figure 6: $|S_{11}|$ when the antenna was flat or bent.

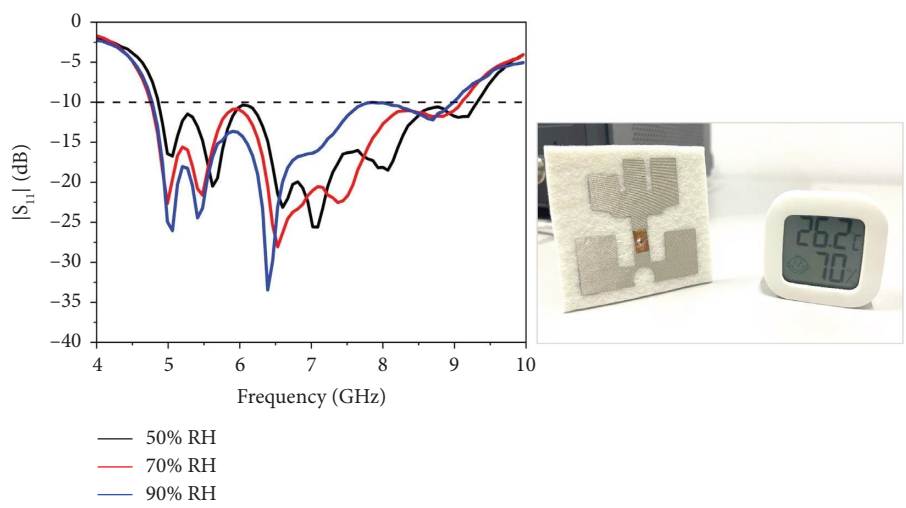

Figure 7: Measured $|S_{11}|$ of antenna at different humidity levels.

absorbs moisture from the air, thus slightly increasing its permittivity. When the antenna was placed on the human arm, its reflection coefficient remained unaltered visibly, indicating that the full ground plane adequately shields the human body.

Wearable antennas are typically integrated onto clothing surfaces. However, human body movements can cause the antenna to bend, crumple, or stretch to varying degrees. For illustrative purposes, bending tests around the x-axis and y-axis were performed. These tests simulate realistic operating condition on an adult arm by wrapping the antenna around a foam cylinder with a 45 mm radius (equivalent to a bending angle of 76.4°). Figure 6 shows the $|S_{11}|$ curves in both the bent and original planar states of the antenna. In the case of bending around y-axis (the green line), the bandwidth remains unchanged, and in the case of bending around x-axis (the red line), the bandwidth decreases slightly. In practice, one can choose the direction of placement of the patch.

The performance of the antenna operating at different humidity levels, i.e., dry condition with a relative humidity (RH) of 50%, moist condition with a RH of 70%, and very damp condition with a RH of 90%, was studied experimentally. The antenna was enclosed in a transparent box to keep the humidity level stable during the measurements. Figure 7 shows the changes in reflection coefficient. As the air humidity increases, the upper bound of the UWB range shifts slightly to lower frequency. It is because the dielectric constant of the substrate increased after absorbing moisture. $|S_{11}|$ increases in higher frequencies in the case of very damp condition but remains under −10 dB, which justifies its robustness in moist conditions.

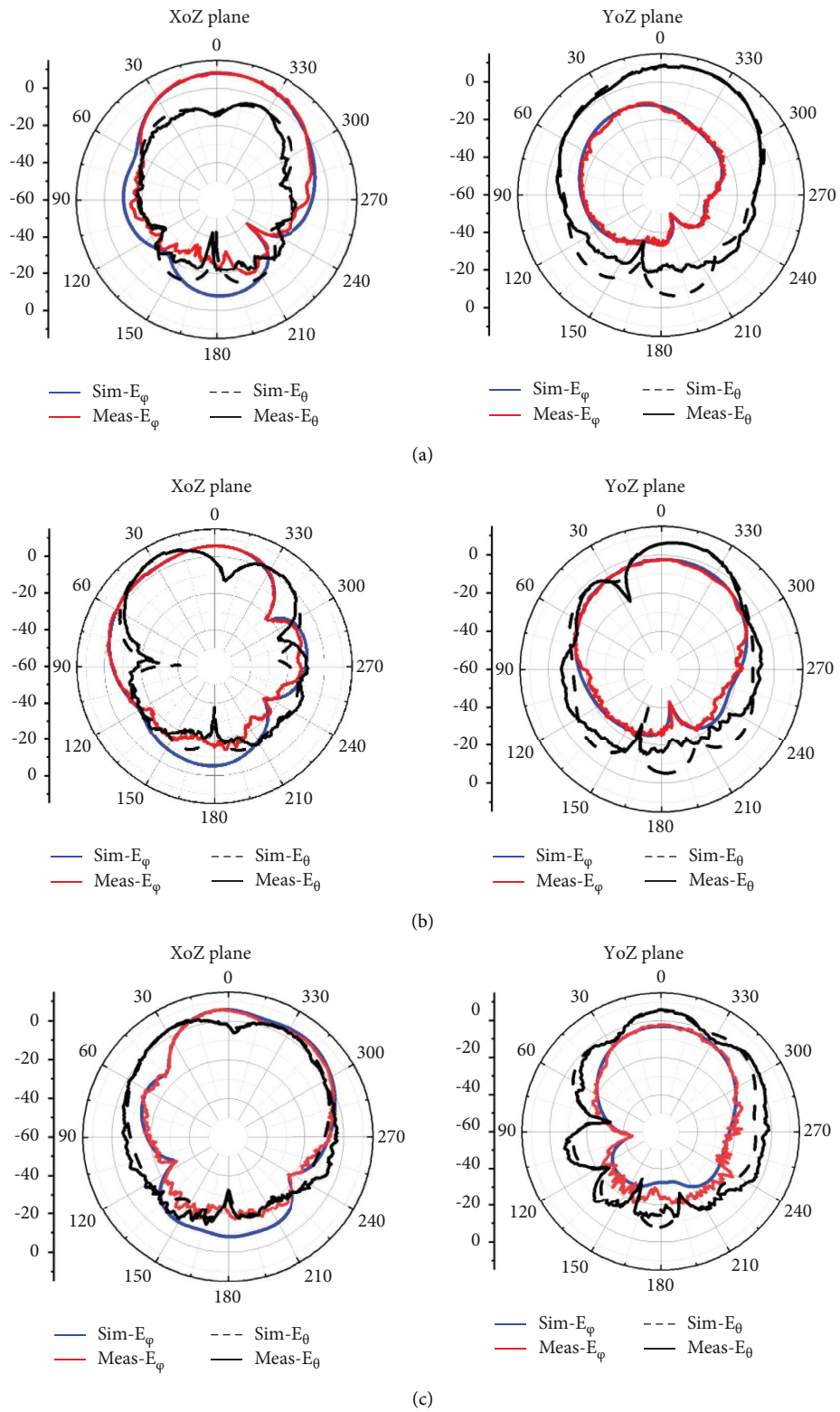

Figure 8: Normalized radiation patterns in free space at (a) 5.06 GHz, (b) 6.49 GHz, and (c) 8.46 GHz.

3.2. Far-Field Characteristics. The far-field radiation of the proposed UWB design was both numerically calculated and measured in an anechoic chamber, as shown in Figures 8(a)–8(c). The simulated and measured radiation patterns at the resonant frequencies of 5.06, 6.49, and 8.46 GHz are in good agreement with each other. Additionally, the antenna exhibits smooth broadside radiation characteristics at all these resonant frequencies, indicating its suitability for off-body

Table 1: Human tissue characteristic parameters at different frequencies.

Human tissue	Frequency (GHz)	Dielectric constant	Electrical conductivity (S/m)	Density (kg/m^3)
Skin	5.06	35.73	3.11	1090
	6.49	34.53	4.33	
	8.46	32.94	6.11	
Fat	5.06	5.02	0.25	930
	6.49	4.89	0.34	
	8.46	4.74	0.46	
Muscle	5.06	49.46	4.11	1050
	6.49	47.56	5.81	
	8.46	45.13	8.17	

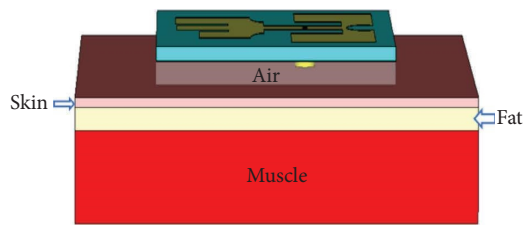

Figure 9: SAR test of the antenna on a simplified human tissue model.

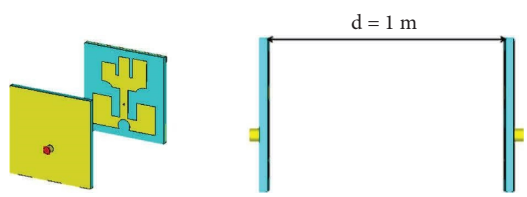

Figure 10: SFF test for the proposed UWB design.

communications in WBANs. The realized gains of the antenna are 9.3, 7.1, and 5.9 dBi by simulation and 9.4, 7.1, and 6.0 dBi by measurement, respectively. The realized gain of the antenna ranges from 5.87 to 10 dBi in the entire passband, with a maximum gain as high as 10 dBi measured at 5.76 GHz. The radiation efficiency of the antenna falls within the range of 78.7% and 84% throughout the operating band.

3.3. Wearing Safety Assessment. The specific absorption ration (SAR) values of the proposed antenna at the resonance frequencies of 5.06, 6.49, and 8.46 GHz were evaluated using CST. The European Union (EU) standard imposes a SAR limit of no more than 2 Watt/kg, averaged over the 10 g of tissue absorbing most of the signal. We used a simplified human model consisting of a 2 mm-thick skin layer, a 5 mm-thick fat layer, and a 20 mm-thick muscle layer, with an overall size of $100 \times 100 \times 27\,\text{mm}^3$. The human tissues' characteristic parameters at different frequencies can be found in [30] and are shown in Table 1. The antenna, with an input power of 0.5 Watt, was placed 5 mm above the human model, as shown in Figure 9. The SAR values calculated according to the EU standard are 0.38 W/kg, 0.23 W/kg, and 0.10 W/kg at 5.06, 6.49, and 8.46 GHz, respectively. These values are far below the EU standard's upper limit and indicate that the antenna design is reliable in terms of safety.

3.4. Time-Domain Performance of the UWB Antenna. An antenna with frequency-domain UWB characteristics may not fully ensure short pulse transmission as it could radiate different frequency components through its different radiating parts or in different directions. This could result in distorted transmitted pulses. The system fidelity factor (SFF) is a measure of the antenna's capability to transmit/receive short pulse signals in the time domain. We conducted SFF tests using CST for both free space and on-body environments. Two identical UWB antennas were positioned facing each other with a distance of 1 m between them. The excitation signal was set as Gaussian form pulse whose frequency spectrum covers the antenna's operating band, as shown in Figure 10. The transmission coefficient ($|S_{21}|$) was numerically calculated, from which we deduced the SFF value. In free space, the SFF value is 0.73, while on the human body, the SFF value is 0.69. The SFF values are higher than the generally acceptable SFF threshold for UWB signal transmission (SFF > 0.5) [31].

Table 2: Performance comparison of the proposed antenna with other state-of-the-art antennas.

Refs	Dielectric material	Dielectric constant	Overall size ($\lambda_g \times \lambda_g$)	BW (GHz)	Gain (dBi)	SAR value (W/kg)	With/without full ground plane
[13]	PDMS	2.85	0.7×0.5	2.2–2.5	3.2–4.5	—	W/O
[14]	LCP	2.9	—	2.5–3.5, 5.1–10.1	0–3.5	4.83	W/O
[15]	Polyester fabric	2.193	0.9×0.6	1.2–4.06	2.8–2.9	—	W/O
[20]	Two-layer felt	1.45	2.3×1.7	3.18–11	1.1–7.2	1.21	W/
[21]	Single-layer PDMS	2.7	3.1×2.6	3.7–10.3	0–4.53	0.17	W/
[22]	Single-layer PDMS	2.77	2.4×2.4	2.85–8.6	2.9–6.2	—	W/
[23]	Single-layer felt	1.45	—	2.9–4.2, 6.5–9.9	4-5	—	W/
[24]	Single-layer felt	1.45	2.7×2.45	3.6–10.3	1.9–7.75	—	W/
[25]	Single-layer PF4 foam	1.06	2×1.75	2.45, 4.5–10	5.8–9.4	0.78	W/
This work	Single-layer felt	1.2	1.6×1.6	4.83–9.57	5.87–10	0.1–0.38	W/

4. Discussion and Comparison

Table 2 presents a comprehensive comparison between our proposed wearable UWB antenna and several representative designs in recent literature. Antennas proposed in [13–15] adopt partial ground plane; as a result, they would have inferior antenna-body isolation performance. Compared to UWB antenna designs in [20–25], our proposed antenna covers the continuous broadband of 4.83–9.57 GHz and has a much higher realized gain, reaching 5.87–10 dBi. Its overall size (in terms of the guided wavelength λ_g) is the smallest. Additionally, the all-textile materials and the single substrate layer jointly ensure low profile, easy integration process, high flexibility, mechanical robustness, and good breathability.

5. Conclusions

A novel single-dielectric-layer all-textile UWB patch antenna with a full ground plane is presented in this paper. The antenna is shaped like the Chinese character "出," which means "Out" or "Send," and exhibits good UWB radiation characteristics. The proposed antenna has low profile, compact size, high flexibility, good breathability, simple structure, and low SAR value. It has the potential for wide range applications in short-range, high-speed WBAN communications.

Data Availability

The data used in this study are available from the corresponding author on reasonable request.

Conflicts of Interest

The authors declare that they have no conflicts of interest.

Acknowledgments

This work was supported partially by the Natural Science Foundation of China (grant nos. 61901253 and 61771300) and partially by the Aeronautical Science Foundation of China (grant no. 202000460S6001).

References

[1] A. Priya, A. Kumar, and B. Chauhan, "A review of textile and cloth fabric wearable antennas," *International Journal of Computer Application*, vol. 116, no. 17, pp. 1–5, 2015.

[2] V. Mishra and A. Kiourti, "Wearable electrically small loop antennas for monitoring joint flexion and rotation," *IEEE Transactions on Antennas and Propagation*, vol. 68, no. 1, pp. 134–141, 2020.

[3] Q. H. Dang, S. J. Chen, D. C. Ranasinghe, and C. Fumeaux, "Modular integration of a passive RFID sensor with wearable textile antennas for patient monitoring," *IEEE Transactions on Components, Packaging, and Manufacturing Technology*, vol. 10, no. 12, pp. 1979–1988, 2020.

[4] R. Joshi, S. K. Podilchak, D. E. Anagnostou et al., "Analysis and design of dual-band folded-shorted patch antennas for robust wearable applications," *IEEE Open Journal of Antennas and Propagation*, vol. 1, pp. 239–252, 2020.

[5] S. Hong, S. H. Kang, Y. Kim, and C. W. Jung, "Transparent and flexible antenna for wearable glasses applications," *IEEE Transactions on Antennas and Propagation*, vol. 64, no. 7, pp. 2797–2804, 2016.

[6] A. Kiourti and J. Volakis, "Colorful textile antennas integrated into embroidered logos," *Journal of Sensor and Actuator Networks*, vol. 4, no. 4, pp. 371–377, 2015.

[7] L. Song, B. Zhang, D. Zhang, and Y. Rahmat-Samii, "Embroidery electro-textile patch antenna modeling and optimization strategies with improved accuracy and efficiency," *IEEE Transactions on Antennas and Propagation*, vol. 70, no. 8, pp. 6388–6400, 2022.

[8] K. Masrakin, H. A. Rahim, P. J. Soh et al., "Assessment of worn textile antennas' exposure on the physiological parameters and well-being of adults," *IEEE Access*, vol. 7, pp. 98946–98958, 2019.

[9] R. Sanchez-Montero, P. L. Lopez-Espi, C. Alen-Cordero, and J. A. Martinez-Rojas, "Bend and moisture effects on the performance of a U- shaped slotted wearable antenna for off-body communications in an industrial scientific medical (ISM) 2.4 GHz band," *Sensors*, vol. 19, no. 8, p. 1804, 2019.

[10] A. Anbalagan, E. F. Sundarsingh, and V. S. Ramalingam, "Design and experimental evaluation of a novel on-body textile antenna for unicast applications," *Microwave and Optical Technology Letters*, vol. 62, no. 2, pp. 789–799, 2019.

[11] H. R. Khaleel, "Design and fabrication of compact inkjet printed antennas for integration within flexible and wearable electronics," *IEEE Transactions on Components, Packaging, and Manufacturing Technology*, vol. 4, no. 10, pp. 1722–1728, 2014.

[12] H. A. Elmobarak Elobaid, S. K. Abdul Rahim, M. Himdi, X. Castel, and M. Abedian Kasgari, "A transparent and flexible polymer-fabric tissue UWB antenna for future wireless networks," *IEEE Antennas and Wireless Propagation Letters*, vol. 16, no. 1, pp. 1333–1336, 2017.

[13] S. R. Zahran, M. A. Abdalla, and A. Gaafar, "New thin wide-band bracelet-like antenna with low SAR for on-arm WBAN applications," *IET Microwaves, Antennas and Propagation*, vol. 13, no. 8, pp. 1219–1225, 2019.

[14] X. Lin, Y. Chen, Z. Gong, B. C. Seet, L. Huang, and Y. Lu, "Ultra-wideband textile antenna for wearable microwave medical imaging applications," *IEEE Transactions on Antennas and Propagation*, vol. 68, no. 6, pp. 4238–4249, 2020.

[15] A. Y. I. Ashyap, S. H. B. Dahlan, Z. Z. Abidin et al., "Robust and efficient integrated antenna with EBG-DGS enabled wide bandwidth for wearable medical device applications," *IEEE Access*, vol. 8, pp. 56346–56358, 2020.

[16] P. Sambandam, M. Kanagasabai, S. Ramadoss et al., "Compact monopole antenna backed with fork-slotted EBG for wearable applications," *IEEE Antennas and Wireless Propagation Letters*, vol. 19, no. 2, pp. 228–232, 2020.

[17] B. S. Cook and A. Shamim, "Utilizing wideband AMC structures for high-gain inkjet-printed antennas on lossy paper substrate," *IEEE Antennas and Wireless Propagation Letters*, vol. 12, no. 1, pp. 76–79, 2013.

[18] X. Liu, Y. Di, H. Liu, Z. Wu, and M. M. Tentzeris, "A planar windmill-like broadband antenna equipped with artificial magnetic conductor for off-body communications," *IEEE Antennas and Wireless Propagation Letters*, vol. 15, no. 1, pp. 64–67, 2016.

[19] T. N. Kapetanakis, C. D. Nikolopoulos, K. Petridis, and I. O. Vardiambasis, "Wearable textile antenna with a graphene

sheet or conductive fabric patch for the 2.45 GHz band," *Electronics*, vol. 10, no. 21, p. 2571, 2021.

[20] L. A. Yimdjo Poffelie, P. J. Soh, S. Yan, and G. A E Vandenbosch, "A high fidelity all-textile UWB antenna with low back radiation for off-body WBAN applications," *IEEE Transactions on Antennas and Propagation*, vol. 64, no. 2, pp. 757–760, 2016.

[21] R. B. V. B. Simorangkir, A. Kiourti, and K. P. Esselle, "UWB wearable antenna with a full ground plane based on PDMS-embedded conductive fabric," *IEEE Antennas and Wireless Propagation Letters*, vol. 17, no. 3, pp. 493–496, 2018.

[22] B. Mohamadzade, R. B. V. B. Simorangkir, R. M. Hashmi, and A. Lalbakhsh, "A conformal ultrawideband antenna with monopole-like radiation patterns," *IEEE Transactions on Antennas and Propagation*, vol. 68, no. 8, pp. 6383–6388, 2020.

[23] P. B. Samal, P. J. Soh, and Z. Zakaria, "Compact microstrip-based textile antenna for 802.15.6 WBAN-UWB with full ground plane," *International Journal of Antennas and Propagation*, vol. 2019, Article ID 8283236, 12 pages, 2019.

[24] P. B. Samal, P. J. Soh, and G. A. E. Vandenbosch, "UWB all-textile antenna with full ground plane for off-body WBAN communications," *IEEE Transactions on Antennas and Propagation*, vol. 62, no. 1, pp. 102–108, 2014.

[25] P. B. Samal, S. J. Chen, and C. Fumeaux, "Wearable textile multiband antenna for WBAN applications," *IEEE Transactions on Antennas and Propagation*, vol. 71, no. 2, pp. 1391–1402, 2023.

[26] S. Sankaralingam and B. Gupta, "Determination of dielectric constant of fabric materials and their use as substrates for design and development of antennas for wearable applications," *IEEE Transactions on Instrumentation and Measurement*, vol. 59, no. 12, pp. 3122–3130, 2010.

[27] H. Tu, Y. Zhang, H. Hong, J. Hu, and X. Ding, "A strip line ring resonator for dielectric properties measurement of thin fabric," *The Journal of The Textile Institute*, vol. 112, no. 11, pp. 1772–1778, 2021.

[28] Saintyear Electronic Inc, *Technical Application Guide: PF39B*, Saintyear Electronic Inc, Hangzhou, China, 2023.

[29] H. Li, J. Du, X.-X. Yang, and S. Gao, "Low-profile all-textile multiband microstrip circular patch antenna for WBAN applications," *IEEE Antennas and Wireless Propagation Letters*, vol. 21, no. 4, pp. 779–783, 2022.

[30] IFAC, "Dielectric properties of body tissues," 2018, http://niremf.ifac.cnr.it/tissprop.

[31] G. Quintero, J. F. Zurcher, and A. K. Skrivervik, "System fidelity factor: a new method for comparing UWB antennas," *IEEE Transactions on Antennas and Propagation*, vol. 59, no. 7, pp. 2502–2512, 2011.